# This paper is published as part of a *PCCP* themed issue on solid state and cluster structure prediction

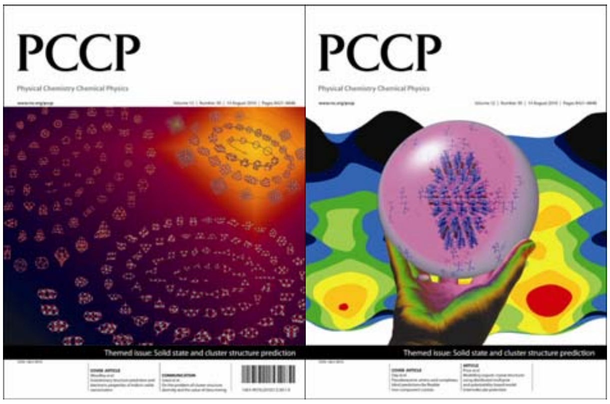


**Guest Editors: Richard Catlow and Scott M. Woodley**

Appearance of bulk-like motifs in Si, Ge, and Al clusters
Wen-Cai Lu, C. Z. Wang, Li-Zhen Zhao, Wei Zhang, Wei Qin and K. M. Ho, *Phys. Chem. Chem. Phys.*, 2010
**DOI:** 10.1039/c004059b

Small germanium sulfide clusters: mass spectrometry and density functional calculations
Joseph J. BelBruno and Andrei Burnin, *Phys. Chem. Chem. Phys.*, 2010
**DOI:** 10.1039/c003704d

Prediction of the structures of free and oxide-supported nanoparticles by means of atomistic approaches: the benchmark case of nickel clusters
Giulia Rossi, Luca Anghinolfi, Riccardo Ferrando, Florin Nita, Giovanni Barcaro and Alessandro Fortunelli, *Phys. Chem. Chem. Phys.*, 2010
**DOI:** 10.1039/c003949g

Crystal structure prediction and isostructurality of three small organic halogen compounds
Aldi Asmadi, John Kendrick and Frank J. J. Leusen, *Phys. Chem. Chem. Phys.*, 2010
**DOI:** 10.1039/c003971c

Aspects of crystal structure prediction: some successes and some difficulties
Michael O'Keeffe, *Phys. Chem. Chem. Phys.*, 2010
**DOI:** 10.1039/c004039h

Nanopolycrystalline materials; a general atomistic model for simulation
Dean C. Sayle, Benoît C. Mangili, David W. Price and Thi X. Sayle, *Phys. Chem. Chem. Phys.*, 2010
**DOI:** 10.1039/b918990d

Isomorphism between ice and silica
Gareth A. Tribello, Ben Slater, Martijn A. Zwijnenburg and Robert G. Bell, *Phys. Chem. Chem. Phys.*, 2010
**DOI:** 10.1039/b916367k

Investigation of the structures and chemical ordering of small Pd–Au clusters as a function of composition and potential parameterisation
Ramli Ismail and Roy L. Johnston, *Phys. Chem. Chem. Phys.*, 2010
**DOI:** 10.1039/c004044d

Predicting crystal structures *ab initio*: group 14 nitrides and phosphides
Judy N. Hart, Neil L. Allan and Frederik Claeyssens, *Phys. Chem. Chem. Phys.*, 2010
**DOI:** 10.1039/c004151c

Zeolitic polyoxometalates metal organic frameworks (Z-POMOF) with imidazole ligands and ε-Keggin ions as building blocks; computational evaluation of hypothetical polymorphs and a synthesis approach
L. Marleny Rodriguez Albelo, A. Rabdel Ruiz-Salvador, Dewi L. Lewis, Ariel Gómez, Pierre Mialane, Jérome Marrot, Anne Dolbecq, Alvaro Sampieri and Caroline Mellot-Draznieks, *Phys. Chem. Chem. Phys.*, 2010
**DOI:** 10.1039/c004234j

# Investigation of the structures and chemical ordering of small Pd–Au clusters as a function of composition and potential parameterisation

**Ramli Ismail and Roy L. Johnston***

***Received 9th March 2010, Accepted 30th June 2010***
***First published as an Advance Article on the web 12th July 2010***
**DOI: 10.1039/c004044d**

The energetics, structures and segregation of Pd–Au nanoalloys (all compositions for 34- and 38-atoms) have been studied using a genetic algorithm global optimization technique with the Gupta empirical potential. Three modifications of the Pd–Au parameters have been studied: parameter set ***I*** in which all parameters ($A$, $\xi$, $p$, $q$ and $r_0$) in the Gupta potential are weighted in a symmetrical fashion; parameter set ***II*** (symmetric weighting of only the pair and many-body energy scaling parameters $A$ and $\xi$); and parameter set ***III*** (antisymmetric weighting of $A$ and $\xi$). Structural analysis reveals competition between a range of structural families; decahedra, polyicosahedra and truncated octahedra (for 34 atoms) and incomplete-icosahedra-Mackay, decahedra, polyicosahedra (low-symmetry), six-fold-polyicosahedra and a mixed octahedron–icosahedron (Oh–Ih) structure (for 38 atoms). It is shown that, by finely tuning the Gupta potential, it is possible to qualitatively reproduce the results observed at higher levels of theory (*e.g.* Density Functional Theory). There are four main types of chemical ordering which are observed: core–shell; spherical cap; ball-and-cup; and mixed. It is shown that the chemical ordering and the proportion of Pd–Au heteronuclear bonds in these clusters are strongly dependent on the potential parameters. Comparison of the results from parameter set ***III*** and two previously fitted potentials shows that the **DFT-fit** potential gives rise to similar results for energies, and lowest energy structures and homotops to those for parameter set ***III*** with $w_a = 0.8$, but the **exp-fit** potential gives rise to qualitatively different results.

## 1. Introduction

There is considerable interest in the chemical and physical properties and potential applications of metal nanoparticles.[1,2] Much of the interest has focused on mono- and bimetallic nanoparticles formed from elements in the nickel and copper groups of the periodic table: Ni, Pd, Pt; Cu, Ag, Au.[3,4] For example, palladium, which has fcc symmetry in the bulk,[5] shows a variety of structures, ranging from fcc cuboctahedra, icosahedra and truncated decahedra to twinned fcc structures for nanoparticles with 1–5 nm diameter. These structures have been produced using either colloidal methods or vapour deposition and have been characterised with the aid of high-resolution electron microscopy (HREM). All structural motifs appear to have very similar energies, so that transitions between different states are possible. Icosahedra are only expected for very small clusters with a high surface to volume ratio, while decahedra and fcc cuboctahedral or truncated octahedral particles are more stable than icosahedra for larger sizes.[6]

Gold clusters have been studied intensively in recent years. The structural size evolution in gold may be described as a sequence of transitions from specific "molecular" structures, at the extremely small size range, with effective cluster diameter $\leq$ 1 nm (40 atoms), to ordered "non-crystallographic" (decahedral) structures at larger sizes, culminating for sizes $>$2 nm ($>$250 atoms) in crystallites of the bulk lattice structure (fcc) with specific faceted morphologies (*i.e.*, variants of truncated octahedra and their twins).[7]

Gold clusters have been grown from metal ions reduced at the oil–water interface in the presence of a surface passivating agent. Observation by HREM shows a variety of structures (decahedron, truncated octahedron, icosahedron, and amorphous) for passivated particles of a few nanometres diameter, with a prevalence, however, of Marks and Ino-decahedra. The smallest fcc clusters observed correspond to the truncated octahedron, whilst at sizes $\sim$15 Å, the Marks decahedron is the most stable motif.[8] Marks-decahedral motifs have also been found as stable structures for 1–2 nm gold clusters by X-ray powder diffraction. Based on atomistic modelling, these were assigned as 75-, 101- and 146-atom clusters.[9]

Among bimetallic nanoclusters ("nanoalloys") the Pd–Au system has been widely studied.[4] In a study by Liu *et al.*, for example, bimetallic Pd–Au nanoclusters have been synthesized by the reduction of metal ions in the presence of a polymer stabilizer. HREM results confirmed three stable configurations: $Pd_{core}Au_{shell}$, random solid solutions and eutectic-like configurations. Coexistence of fcc-like and multiple twinned (octahedral and decahedral) structures was found because of the close separation of energies between these structures. Although $Pd_{core}Au_{shell}$ structures are stable at low temperature, inversion to the $Au_{core}Pd_{shell}$ structure was observed upon heating to approximately 500 K.[10]

*School of Chemistry, University of Birmingham, Edgbaston, Birmingham, B15 2TT, United Kingdom.*
*E-mail: r.l.johnston@bham.ac.uk; Tel: +44(0)121 414 7477*

Pd–Au clusters are of great interest to theoretical and experimental researchers because of their interesting properties that are not found for the respective pure metals. The electronic structures of Pd–Au clusters are quite distinct from Pd or Au, due to their differing atomic electron configurations and electronegativities.[4] Nanoclusters of Pd–Au supported on a variety of surfaces (*e.g.* magnesia, titania, silica, alumina) show great potential for a wide range of catalytic reactions, such as: acetylene cyclotrimerization (to yield benzene) and related reactions;[13] selective hydrogenation;[14–16] hydrodechlorination of trichloroethene in water at room temperature;[17] low-temperature synthesis of hydrogen peroxide from oxygen and hydrogen,[18,19] CO and alcohol reduction;[20] the Sonagashira cross-coupling reaction;[21] and synthesis of vinyl acetate by acetoxylation of ethylene.[22,23]

In this paper, the energetics, structures and segregation (chemical ordering) of Pd–Au nanoalloys are investigated as a function of composition for 34- and 38-atom clusters, using a genetic algorithm for global geometry optimisation (*i.e.* global energy minimisation) of the clusters and with the interatomic interactions described by the Gupta many-body potential. We also present a detailed study of how the structures and chemical ordering displayed by these nanoalloys change when the heteronuclear potential parameters are varied systematically. The analysis is aided by the calculation of excess (mixing) energies, average nearest-neighbour distances and a chemical ordering parameter.

The reason for concentrating here on 34- and 38-atom clusters, is that our previous work on Pd–Au (and other nanoalloy systems)[11,24–26] have shown that 34-atom clusters typically exhibit a wide range of structural motifs as a function of composition, while 38-atom clusters (for which truncated octahedral structures typically dominate) are of interest for testing how different chemical orderings are stabilised by different heteroatomic interaction strengths.

## 2. Theoretical methods

### 2.1 The Gupta potential

The Gupta potential, used to model inter-atomic interactions in metal systems,[12,27] is a semi-empirical potential derived within the tight-binding second-moment approximation. The configurational energy of a cluster is written as the sum over all the atoms of attractive and repulsive energy components:

$$V_{\text{clus}} = \sum_{i}^{N} \{V^r(i) - V^m(i)\} \quad (1)$$

where the Born–Mayer pair repulsive term $V^r(i)$ is expressed as:

$$V^r(i) = \sum_{j\neq i}^{N} A(\alpha,\beta)\exp\left\{-p(\alpha,\beta)\left(\frac{r_{ij}}{r_0(\alpha,\beta)}-1\right)\right\} \quad (2)$$

and the many-body attractive term $V^m(i)$ is expressed as:

$$V^m(i) = \sqrt{\sum_{j\neq i}^{N} \xi^2(\alpha,\beta)\exp\left\{-2q(\alpha,\beta)\left(\frac{r_{ij}}{r_0(\alpha,\beta)}-1\right)\right\}} \quad (3)$$

In eqn (2) and (3), $\alpha$ and $\beta$ represent the atomic species of atoms $i$ and $j$, respectively. $A$, $\xi$, $p$ and $q$ are the potential parameters that are usually fitted to experimental properties of bulk metals and alloys, such as the cohesive energy, lattice parameters, and independent elastic constants for the reference crystal structure at 0 K. $r_0$ denotes the nearest-neighbour distance of the pure bulk elements, often taken as the average of the pure distances, but it can also be taken as the experimental nearest-neighbour distance in some specific ordered bulk alloy. $r_{ij}$ is the distance between atoms $i$ and $j$.

Values of the Gupta potential parameters describing Pd–Pd and Au–Au interactions, taken from the work of Cleri and Rosato,[12] are listed in Table 1, along with three alternative sets of Pd–Au parameters considered in a previous study by Pittaway *et al.*[11]

### 2.2 Parameterisations of the Gupta potential

A study of Pd–Pt clusters by Massen *et al.*[28] concluded that parameters obtained by averaging the parameters of elemental Pd and Pt, gave a good qualitative fit to previous experimental and theoretical studies of Pd–Pt bimetallic clusters.[29–31] A more detailed investigation of the effect on structure and chemical ordering of varying the heteronuclear (Pd–Pt) parameters for 34-atom Pd–Pt clusters gave more decahedral motifs for Pd–Pt parameters which are slightly biased towards the weaker Pd–Pd interaction,[24] which is consistent with DFT results.[26] These parameters still favour core–shell ordering, as for the average potential. Recent GA calculations for 34- and 38-atom Pd–Pt clusters have shown that the heteronuclear parameters for a new Gupta potential (fitted to DFT calculations on pure metals and alloy solids)[32] lie slightly to the weaker bonding (*i.e.* closer to the Pd–Pd parameters) side of the average.[33] The calculated excess energies and structural motifs are consistent with this.

DFT calculations of small Pd, Au and Pd–Au (1 : 1 composition) clusters (2–20 atoms), have shown that the mixed clusters have binding energies which are intermediate between those of Pd and Au, but are biased towards Pd, indicating that the Pd–Au bonding is greater than the average of Pd–Pd and Au–Au.[33]

In this study, the heteronuclear Pd–Au Gupta potential parameters $\{P\}$ are derived as the weighted average of the corresponding pure metal Pd–Pd and Au–Au parameters:[24]

$$P(\text{Pd–Au}) = w_1P(\text{Pd–Pd}) + w_2P(\text{Au–Au}) \quad (4)$$

where $w_1 + w_2 = 1$. Weighting parameters have been investigated in the range $0 \leq w \leq 1$, in steps $\Delta w = 0.1$. The following parametrisations have been studied.

**Parameter set *I*.** All the Pd–Au Gupta potential parameters $\{P\} = \{A, \xi, p, q \text{ and } r_0\}$ are obtained as:

$$P(\text{Pd–Au}) = wP(\text{Pd–Pd}) + (1 - w)P(\text{Au–Au}) \quad (5)$$

This is symmetrical weighting of all parameters, since all of the parameters vary in the same sense—*i.e.* from the value for Au–Au (for $w = 0$) to the value for Pd–Pd (for $w = 1$).

 

**Table 1** Comparison of the **average**, **DFT-fit** and **exp-fit** Gupta potential parameters.[11] For the **average** potential, the homonuclear parameters are taken from Cleri and Rosato,[12] while in the other potentials they are fitted along with the heteronuclear parameters

| | Pd–Pd | | | Au–Au | | | Pd–Au | | |
|---|---|---|---|---|---|---|---|---|---|
| Parameter | **average** | **DFT-fit** | **exp-fit** | **average** | **DFT-fit** | **exp-fit** | **average** | **DFT-fit** | **exp-fit** |
| $A$/eV | 0.1746 | 0.1653 | 0.171493044 | 0.2061 | 0.2091 | 0.209570656 | 0.19 | 0.1843 | 0.2764 |
| $\xi$/eV | 1.718 | 1.6805 | 1.701873210 | 1.79 | 1.8097 | 1.815276400 | 1.75 | 1.7867 | 2.082 |
| $p$ | 10.867 | 10.8535 | 11.000 | 10.229 | 10.2437 | 10.139 | 10.54 | 10.5420 | 10.569 |
| $q$ | 3.742 | 3.7516 | 3.794 | 4.036 | 4.0445 | 4.033 | 3.89 | 3.8826 | 3.913 |
| $r_0$/Å | 2.7485 | 2.7485 | 2.7485 | 2.884 | 2.8840 | 2.884 | 2.816 | 2.8160 | 2.816 |

In parameter sets ***II*** and ***III***, instead of weighting all the parameters in the Gupta potential only the $A$ (pair repulsion) and $\xi$ (many-body) parameters were varied with parameters $p$, $q$ and $r_0$ being fixed at their arithmetic mean values ($w = 0.5$).

**Parameter set *II*.** As for parameter set ***I***, parameters $A$ and $\xi$ are varied in the same sense ("symmetric"), with the weighting factor being denoted $w_s$:

$$A(\text{Pd–Au}) = w_s A(\text{Pd–Pd}) + (1 - w_s)A(\text{Au–Au}) \quad (6)$$

$$\xi(\text{Pd–Au}) = w_s\xi(\text{Pd–Pd}) + (1 - w_s)\xi(\text{Au–Au}) \quad (7)$$

Comparison of the results for parameter sets ***I*** and ***II*** will enable us to judge the importance of the energy scaling parameter ($A$ and $\xi$) compared to the range exponents ($p$ and $q$).

**Parameter set *III*.** In contrast to parameter set ***II***, parameters $A$ and $\xi$ are varied in the opposite sense ("antisymmetric"—*i.e.* as $A$ varies between the limits of the values for Pd–Pd and Au–Au, $\xi$ varies in the opposite direction), with the weighting factor being denoted $w_a$:

$$A(\text{Pd–Au}) = w_a A(\text{Pd–Pd}) + (1 - w_a)A(\text{Au–Au}) \quad (8)$$

$$\xi(\text{Pd–Au}) = (1 - w_a)\xi(\text{Pd–Pd}) + w_a\xi(\text{Au–Au}) \quad (9)$$

The reason for investigating parameter set ***III*** is that it allows regions of Pd–Au parameter space to be explored which have: (i) low $A$ and high $\xi$ values, corresponding to strong Pd–Au bonding; and (ii) high $A$ and low $\xi$, corresponding to weak Pd–Au bonding.

The parameter values for parameter sets ***I***, ***II*** and ***III*** are all listed in Table 2.

In this study, the results obtained for parameter sets ***I–III*** have also been compared with those reported by Pittaway *et al.*[11] using the Pd–Au heteronuclear parameters that were fitted to the results of first-principles Density Functional Theory (DFT) calculations[11] ("**DFT-fit**") and those fitted to experimental properties of bulk Pd, Au and Pd–Au alloys[34] ("**exp-fit**"), as listed in Table 1. It should be noted that the "**average**" (arithmetic mean) potential previously reported,[11,25,26] corresponds to $w = 0.5$ (set ***I***), $w_s = 0.5$ (***II***) and $w_a = 0.5$ (***III***).

## 2.3 The Birmingham cluster genetic algorithm (BCGA)

The Birmingham Cluster Genetic Algorithm (BCGA) program, which has been described elsewhere,[35] was used to find the putative global minima (GM) and other low-lying energy minima of 34- and 38-atom Pd–Au clusters, for all compositions. The BCGA parameters used in this work were: population size = 40 clusters; crossover rate = 80% (*i.e.*, 32 offspring are produced per generation); crossover type = 1-point weighted cut-and-splice (the cut position is calculated based on the fitness values of the parents); selection = roulette wheel; mutation rate = 0.1; mutation type = mutate_move; maximum number of generations = 400. 100 GA runs were performed for each composition. The GA was terminated when the population was found to have converged for 10 consecutive generations.

**Table 2** The potential parameters for parameter set: ***I*** [symmetric weighting ($w$) of all parameters]; ***II*** [symmetric weighting ($w_s$) of $A$ and $\xi$]; and ***III*** [antisymmetric weighting ($w_a$) of $A$ and $\xi$]

| **Set** | $w$ | **0.0** | **0.1** | **0.2** | **0.3** | **0.4** | **0.5** | **0.6** | **0.7** | **0.8** | **0.9** | **1.0** |
|---|---|---|---|---|---|---|---|---|---|---|---|---|
| **I** | $A$ | 0.2061 | 0.2030 | 0.1998 | 0.1967 | 0.1935 | 0.1904 | 0.1872 | 0.1841 | 0.1809 | 0.1778 | 0.1746 |
| | $\xi$ | 1.7900 | 1.7828 | 1.7756 | 1.7684 | 1.7612 | 1.7540 | 1.7468 | 1.7396 | 1.7324 | 1.7252 | 1.7180 |
| | $p$ | 10.2290 | 10.2928 | 10.3566 | 10.4204 | 10.4842 | 10.5480 | 10.6118 | 10.6756 | 10.7394 | 10.8032 | 10.8670 |
| | $q$ | 4.0360 | 4.0066 | 3.9772 | 3.9478 | 3.9184 | 3.8890 | 3.8596 | 3.8302 | 3.8008 | 3.7714 | 3.7420 |
| | $r_0$ | 2.8840 | 2.8705 | 2.8569 | 2.8434 | 2.8298 | 2.8163 | 2.8027 | 2.7892 | 2.7756 | 2.7621 | 2.7485 |
| | $w_s$ | **0.0** | **0.1** | **0.2** | **0.3** | **0.4** | **0.5** | **0.6** | **0.7** | **0.8** | **0.9** | **1.0** |
| **II** | $A$ | 0.2061 | 0.2030 | 0.1998 | 0.1967 | 0.1935 | 0.1904 | 0.1872 | 0.1841 | 0.1809 | 0.1778 | 0.1746 |
| | $\xi$ | 1.7900 | 1.7828 | 1.7756 | 1.7684 | 1.7612 | 1.7540 | 1.7468 | 1.7396 | 1.7324 | 1.7252 | 1.7180 |
| | $p$ | | | | | | 10.5480 (fixed at average) | | | | | |
| | $q$ | | | | | | 3.8890 (fixed at average) | | | | | |
| | $r_0$ | | | | | | 2.8163 (fixed at average) | | | | | |
| | $w_a$ | **0.0** | **0.1** | **0.2** | **0.3** | **0.4** | **0.5** | **0.6** | **0.7** | **0.8** | **0.9** | **1.0** |
| **III** | $A$ | 0.2061 | 0.2030 | 0.1998 | 0.1967 | 0.1935 | 0.1904 | 0.1872 | 0.1841 | 0.1809 | 0.1778 | 0.1746 |
| | $\xi$ | 1.7180 | 1.7252 | 1.7324 | 1.7396 | 1.7468 | 1.7540 | 1.7612 | 1.7684 | 1.7756 | 1.7828 | 1.7900 |
| | $p$ | | | | | | 10.5480 (fixed at average) | | | | | |
| | $q$ | | | | | | 3.8890 (fixed at average) | | | | | |
| | $r_0$ | | | | | | 2.8163 (fixed at average) | | | | | |

### 2.4 Energetic analysis

When studying fixed-size bimetallic clusters, the excess (or mixing) energy as a function of composition, $\Delta_N^{\text{Gupta}}$, is a useful quantity. For binary nanoalloys with fixed size ($N$ = 34 or 38 atoms) but different compositions, $\Delta_N^{\text{Gupta}}$ is defined as

$$\Delta_N^{\text{Gupta}} = E_N^{\text{Gupta}}(A_M B_{N-M}) - M\frac{E_N^{\text{Gupta}}(A_N)}{N} - (N-M)\frac{E_N^{\text{Gupta}}(B_N)}{N} \tag{10}$$

where $E_N^{\text{Gupta}}(A_M B_{N-M})$ is the total energy of a given cluster calculated at the Gupta level and $E_N^{\text{Gupta}}(A_M)$ and $E_N^{\text{Gupta}}(B_N)$ are the total energies of the GM of the pure metal clusters (*i.e.* $Pd_N$ and $Au_N$). This excess energy is an unbiased quantity, defined as zero for the global minima of the pure clusters. Negative values of $\Delta_N^{\text{Gupta}}$ indicate that mixing is favourable.

### 2.5 Pair distribution function (PDF) and average nearest-neighbour distance (ANND)

For quantitative purposes, it is appropriate to calculate the **pair distribution function (PDF)**, $g_p(r)$ as follows:

$$g_p(r) = \frac{V}{N^2}\left\langle \sum_i^N \sum_{j\neq i}^N \delta\left[r - r_{ij}\right]\right\rangle \tag{11}$$

where $N$ is the total number of atoms, $V$ is the volume, $r_{ij}$ denotes the distance between atoms $i$ and $j$, and the brackets represent a time average. The $g_p(r)$ function gives the probability of finding an atom of any type at a distance $r$, and it allows characterization of the lattice structure during the generation of the nanoalloy.[36]

From $g_p(r)$, the **average nearest-neighbour distance (ANND)** can be defined as:

$$\text{ANND} = \frac{\int_0^{r_c} rg(r)4\pi r^2 \mathrm{d}r}{\int_0^{r_c} g(r)4\pi r^2 \mathrm{d}r} \tag{12}$$

where the cut-off $r_c$ is chosen to be half way between the average nearest- and second-nearest-neighbour distances in the cluster.[37] This term can be simplified as the sum of the nearest neighbour atomic distances divided by the number of bonds in the cluster.[38]

### 2.6 Chemical ordering

Binary nanoalloys generally present more complex structures than monometallic clusters and global optimisation is more difficult due to the existence of homotops,[39] which are isomers with the same geometry and composition but with a different arrangement of the two types of atoms.

For an A–B alloy system, the chemical order parameter, $\sigma$ is defined as;

$$\sigma = \frac{N_{A-A} + N_{B-B} - N_{A-B}}{N_{A-A} + N_{B-B} + N_{A-B}} \tag{13}$$

where $N_{A-B}$ is the number of nearest-neighbour $A$–$B$ bonds and $N_{A-A}$ and $N_{B-B}$ denote the numbers of homonuclear bonds in the binary cluster. The $\sigma$ value is positive when phase separation (segregation) takes place, close to zero when disordered mixing occurs, and negative when there is more ordered mixing (including layering and onion-like configurations).[40]

## 3. Results and discussion

### 3.1 34-Atom palladium–gold clusters

This study produced results which corroborate those obtained previously, using the **average**, **exp-fit** and **DFT-fit** Gupta parameters,[11] that incomplete decahedral (Dh) structures dominate as the putative GM for 34-atom Pd–Au clusters. In this study, for parameter sets ***I–III***, in addition to the Dh motif, polyicosahedral (pIh)[41] and truncated octahedral (TO) structures (Fig. 1) were also found to be stable structures in GA searches. However, none of the parameterisations gave rise to the decahedron with a close-packed double tetrahedral core [Dh-cp (DT)] motif that is found as the GM for 34-atom Pd–Pt clusters across a wide composition range according to Density Functional Theory (DFT) studies,[26] even after exhaustive searching (500 GA runs).

**Energetics and structural motifs.** Fig. 2 shows the variation of the Gupta excess energy $\Delta_{34}^{\text{Gupta}}$ as a function of composition and weighting parameter, for parameter sets ***I–III***. Fig. 2(a) shows that for set ***I*** all weighting factors ($w$) give rise to negative excess energies, for all compositions, indicating that mixing is favourable. The GM structures of the clusters are dominated by Dh, with several Au-rich pIh ($N_{\text{Au}}$ = 31–33) and TO ($N_{\text{Au}}$ = 24–26) found for Pd-biased parameters ($w$ = 0.8–1.0). On the other hand, changing just $A$ and $\xi$ symmetrically (parameter set ***II***) gives a distinctly different pattern of excess energies, as shown in Fig. 2(b), where some Pd-rich compositions do not favour mixing (excess energies are positive) at $w_s$ = 0.0 ($N_{\text{Au}}$ = 1–3) and $w_s$ = 0.1 ($N_{\text{Au}}$ = 1). The minima in the excess energy curves deepen to a more negative value at $w_s$ = 1.0, but the structural motifs are consistent with those from set ***I***.

Fig. 2(c) shows that endothermic (positive) excess energies ($w_a$ = 0.0–0.3 and partially for $w_a$ = 0.4) are calculated for weighting set ***III***, which may be explained by the fact that $\xi_{\text{PdAu}} \to \xi_{\text{Pd}}$ and $A_{\text{PdAu}} \to A_{\text{Pd}}$. Another important finding is that the lowest excess energy (at $w_a$ = 1.0) for this set is −7.1647 eV, which is considerably larger than the values of

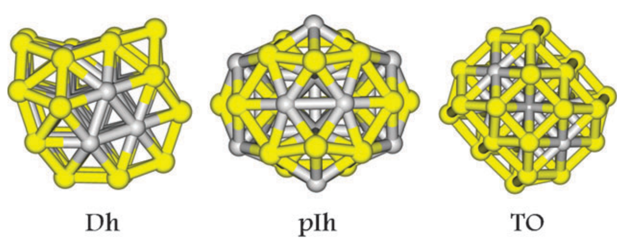


**Fig. 1** GM Structural motifs found for PdAu-34. Au and Pd atoms are denoted by yellow and grey colours, respectively, here and in subsequent figures.

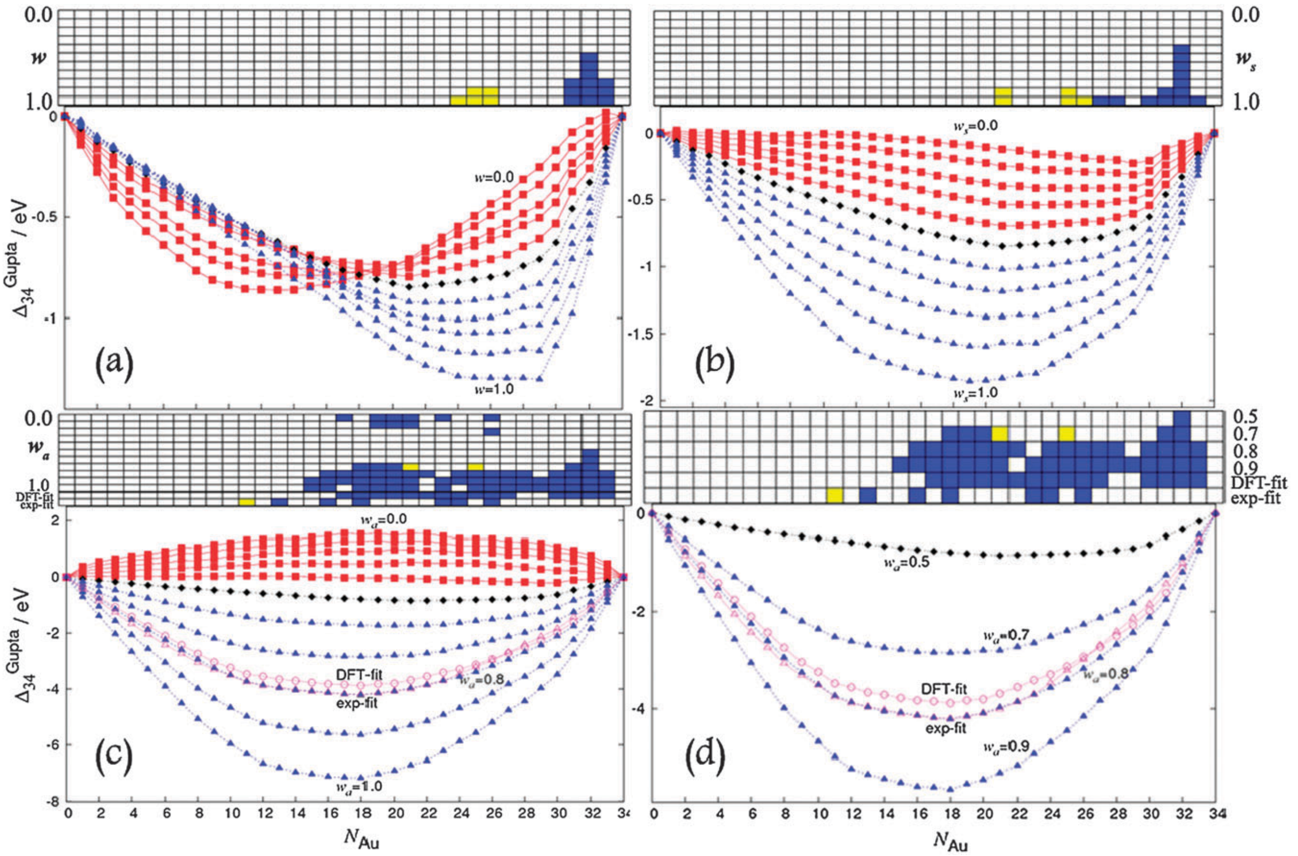


**Fig. 2** (Bottom) Excess energy variation ($\Delta_{34}^{\mathrm{Gupta}}$) for 34-atom Pd–Au clusters using parameter sets ***I*** (a), ***II*** (b), and ***III*** (c). (d) is a comparison between set ***III*** ($w_a$ = 0.5,0.7–0.9) and the **DFT-fit** and **exp-fit** potentials. (Top) GM Structural motifs found, as a function of composition (number of Au atoms) and weighting factor ($w$, $w_s$ or $w_a$): Dh (white); pIh (blue); TO (yellow).

−1.3026 eV (set ***I***) and −1.85515 eV (set ***II***). Generally, we can see that for Pd-rich compositions, Dh structures are the lowest in energy, while for the Au-rich compositions Dh and pIh structures compete, with pIh prevailing as $w_a \rightarrow 1.0$ and TO are only the GM at $w_a = 0.7$, for compositions (13,21) and (9,25).

Observation of pIh structures as the GM for Au-rich compositions in the range $w$ = 0.5–0.8 in Fig. 2(a) (parameter set ***I***) and $w_s$ = 0.4–0.8 in Fig. 2(b) (parameter set ***II***) shows that the variation of structures for these parameter sets is dominated by composition dependence. However, extremely biased weighting shows no more pIh (for low $w$ and $w_s$) and the occurrence of TO as GM (for high $w$ and $w_s$), indicating that there is some dependence on parameterisation for these weighting schemes. In contrast, parameterisation effects clearly dominate composition effects in Fig. 2(c) (parameter set ***III***), in which pIh structures are predicted as putative GM for a wider range of compositions at both low and high $w_a$.

The differences between parameter set ***III*** (for $w_a$ = 0.5 and 0.7–0.9) and the parameters of the fitted (**DFT-fit** and **exp-fit**) potentials are shown in Fig. 2(d). As noted above, $w_a$ = 0.5 is the **average** potential that has previously been used in generating cluster structures for Pd–Au clusters.[11,24–26] The range of $w_a$ = 0.7–0.9 is chosen due to the interesting results at this weighting, having excess energies and structural motifs close to the fitted potentials. From Table 1, the parameters of the **DFT-fit** potential have the following characteristics which are similar to those in set ***III*** (Table 2): $A_{\mathrm{DFT\text{-}fit}}$ (0.1843) $\sim A_{w_a=0.7}$ (0.1841); and $\xi_{\mathrm{DFT\text{-}fit}}$ (1.7867) $\sim \xi_{w_a=0.9}$ (1.7828). Parameter set ***III*** with $w_a > 0.5$ gives stronger Pd–Au bonding, as shown by the more negative excess energies. These parameters correspond to less repulsion ($A_{\mathrm{PdAu}} \rightarrow A_{\mathrm{Pd}}$) and more attraction ($\xi_{\mathrm{PdAu}} \rightarrow \xi_{\mathrm{Au}}$). This is because $A_{\mathrm{Pd}}$ (0.1746) < $A_{\mathrm{Au}}$ (0.2061) and $\xi_{\mathrm{Pd}}$ (1.7180) < $\xi_{\mathrm{Au}}$ (1.7900); and $w_a \rightarrow 1.0$ will reduce $A$ (repulsion) and increase $\xi$ (attraction). On the other hand, the **exp-fit** potential has $A$ (0.2764) and $\xi$ (2.082) parameters which are out of the range of Pd and Au parameters, both being greater than the corresponding Au parameters ($A$ = 0.2096, $\xi$ = 1.8153).[11]

Comparing the excess energy plots in Fig. 2(d), it can be seen that the **DFT-fit** potential curve lies between those of parameter set ***III*** with $w_a$ = 0.7 and 0.8. For the **exp-fit** potential, the plot overlaps with that for $w_a$ = 0.8, especially for mid-range compositions. The excess energies of the GM obtained for the **exp-fit** parameters are more negative than those obtained for the **average** parameters but only slightly more negative than for the **DFT-fit** potential, indicating that Pd–Au mixing is preferred (at the empirical potential level) in this size regime. This highly exothermic mixing is similar to the energy curves obtained for 34-atom Pd–Pt clusters with parameters weighted toward the strongest (Pt–Pt) homonuclear interactions.[11,24]

GM cluster structures for the **DFT-fit** potential are similar to those for parameter set ***III*** for $w_a = 0.8$ and 0.9, with competition between Dh and pIh motifs. However, for the **exp-fit** potential, the GM structures do not match with any weighting ($w_a$) for set ***III***. As for $w_a = 0.7$, a TO GM was found, but at a completely different composition (23,11).

**GM structural variation and segregation profiles.** Fig. 3 shows the structures of the lowest energy PdAu-34 clusters found for parameter sets ***I***, ***II*** and ***III***. The lowest energy structure for set ***I*** (Fig. 3(a)) changes from Dh ($w$ = 0.0–0.8) to TO ($w$ = 0.9) and pIh ($w$ = 1.0). For set ***II*** (Fig. 3(b)), the GM structures for all weighting factors are Dh, changing from Marks-Dh ($w_s$ = 0.0–0.7) to mixed Dh-Ih ($w_s$ = 0.8–1.0). For set ***III*** (Fig. 3(c)), all compositions show positive excess energies for $w_a$ = 0.0–0.3, so the structures selected are the compositions with the most positive excess energies. These structures change from low-symmetry pIh [pIh(LS)] ($w_a$ = 0.0–0.1), to Dh ($w_a$ = 0.2–0.5), mixed Dh-Ih ($w_a$ = 0.6) and pIh ($w_a$ = 0.7–1.0).

Fig. 3(d) shows that the lowest energy structures for both the **DFT-fit** and **exp-fit** potentials occur at composition $Pd_{16}Au_{18}$, which is a similar composition to those found for all minima for set ***III*** ($w_a$ = 0.7–1.0) with $A_{PdAu} \rightarrow A_{Pd-Pd}$ and $\xi_{PdAu} \rightarrow \xi_{Au-Au}$. These structures are pIh with excess energies of −3.8828 and −4.2045 eV, for the **DFT-fit** and **exp-fit** potentials, respectively. Meanwhile, the minima for set ***III*** potentials are −2.8464 ($w_a = 0.7$), −4.2170 ($w_a = 0.8$) and −5.6482 eV ($w_a = 0.9$), all with the same structure. Even though all the minima belong to the same structural family, there are slight differences, particularly for the **exp-fit** potential, where two square faces (for set ***III*** with $w_a = 0.8$ and for **DFT-fit**) expand to become a hexagonal plane and where only 12 (rather than 13) Au atoms lie on the surface. As reported earlier, the structures derived from both fitted potentials tend to maximize the number of Pd–Au bonds; hence, they tend to form incomplete icosahedra or pIh.[11]

There are a number of experimental results[10,42–44] and theoretical calculations[11,25,42,45,46] which indicate the prevalence of $Pd_{core}Au_{shell}$ ordering and are consistent with the lower heat of formation, compared to inverse $Au_{core}Pd_{shell}$ and other configurations.[10] Core–shell segregation is also favoured by: the lower surface energy of Au (Au = 96.8 meV Å$^{-2}$ *vs.* Pd = 131 meV Å$^{-2}$—forming a surface shell of atoms with the lower surface energy lowers the overall cluster surface energy[47,48]); the higher cohesive energy of Pd (Au = 3.81 eV/atom *vs.* Pd = 3.89 eV/atom[49]—maximizing the number of stronger Pd–Pd bonds) and the smaller atomic radius of Pd (Pd = 1.375 Å *vs.* Au = 1.44 Å[49]—a Pd core minimizes bulk elastic strain).

In this work, calculations on 34-atom Pd–Au clusters corroborated the prevalence of core–shell phase segregation behaviour (Fig. 4). When there are a limited number of Au atoms on the surface, three types of incomplete core–shell configurations are observed: ***incomplete core–shell type-A*** (i-CS(A)—having Au atoms occupying low-coordinate surface sites); ***incomplete core–shell type-B*** (i-CS(B)—having a uniform partial monolayer coverage of the surface); and ***incomplete core–shell type-C*** (i-CS(C)—having an intermixed surface). The Au atoms in the i-CS(A) and i-CS(C) configurations occupy the surface sites with the lowest coordination (edge and corner sites) of the Dh, leaving isolated Pd atoms on the higher-coordination surface sites. This segregation is also adopted in AgCu-34 clusters, where Ag atoms occupy the low coordination surface sites.[49]

In addition to core–shell configurations, varying the potential parameters can result in low (spherical cap (layered)

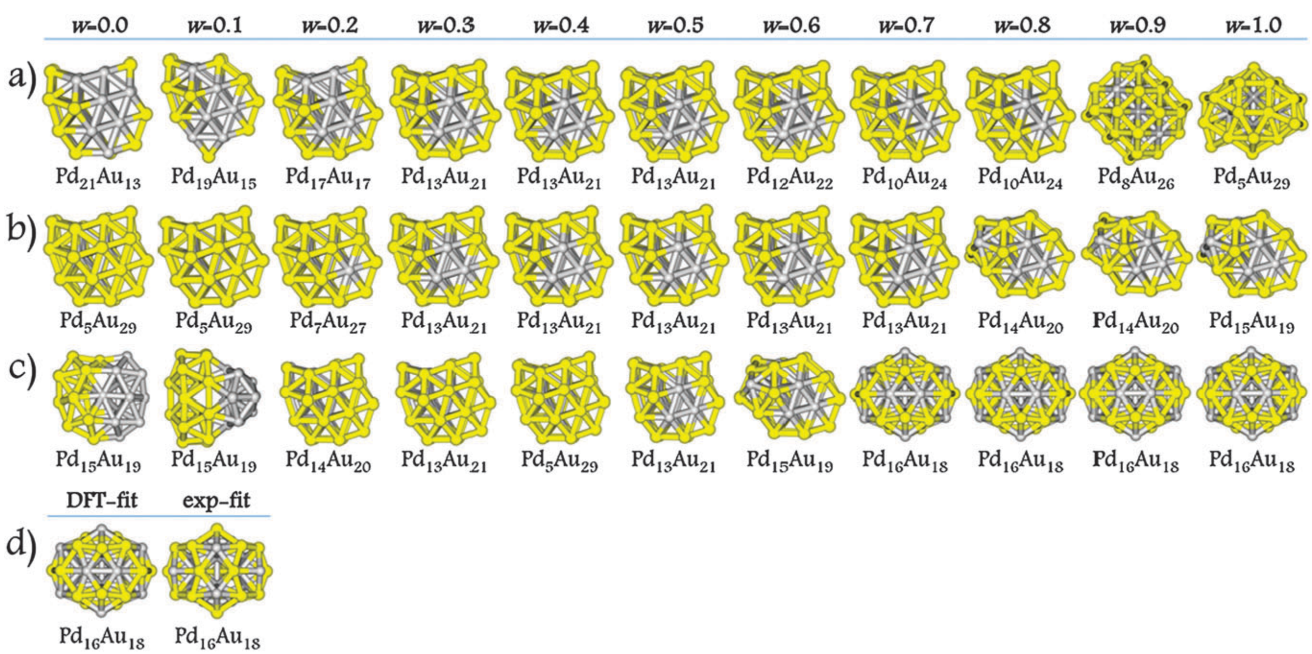


**Fig. 3** Structural variation of the lowest excess energy PdAu-34 isomers found for parameter sets ***I*** (a), ***II*** (b), ***III*** (c), and the **DFT-fit** and **exp-fit** potentials (d).

 

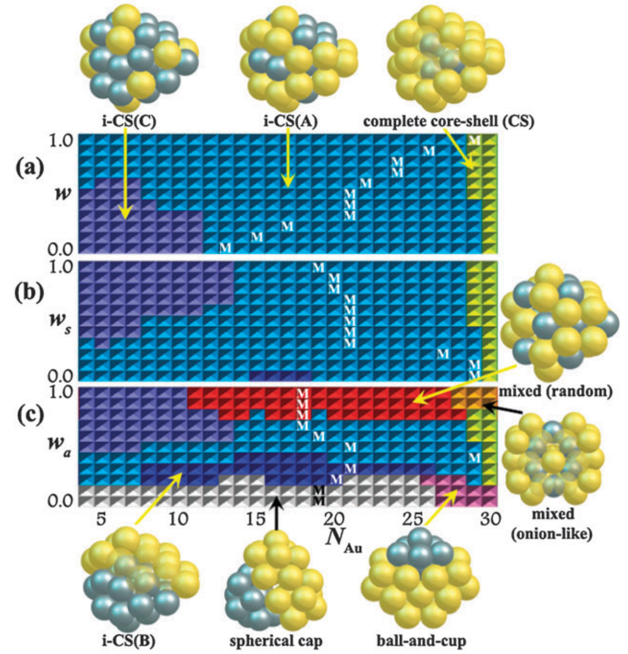


**Fig. 4** Segregation profiles of PdAu-34 using parameter sets ***I*** (a), ***II*** (b), and ***III*** (c).

configurations) to high (mixed configurations) degrees of intermixing, especially for parameter set ***III***. Au-rich compositions with parameter sets ***I***, ***II*** and ***III*** (mid to high $w_a$) possess complete core–shell configurations at $N_{Au}$ = 29/30 (for Dh), but at low $w_a$ (0.0–0.2) the GM with the same compositions adopt ''ball-and-cup'' segregation. Compared to core–shell, the ball-and-cup configurations have several exposed Pd atoms and a preponderance of surface Au atoms on one side, making the ''core'' of Pd atoms off-centre, corresponding to an intermediate segregation between core–shell and spherical cap. This configuration was previously reported for PdPt-34 by Paz-Borbón *et al.*[24]

In contrast to Pd–Pt systems,[24] no evidence of complex crossover between chemical ordering types was detected especially in the medium composition range for parameter set ***I*** (Fig. 4(a)). A possible explanation for this might be the small difference between the $A$ and $\xi$ values of Pd–Pd and Au–Au (Table 1), leading to dominant i-CS(A) and i-CS(C) segregation over the entire weighting and composition range. It is possible to hypothesise that the Pd–Pt situation is more likely to occur for the systems Ag–Au, Ag–Pt and Au–Cu, which all have more widely differing elemental potential parameters.[12,50] While parameter set ***II*** (Fig. 4(b)) also showed a prevalence of i-CS(A) and i-CS(C) configurations, at $w_s$ = 0.0 the GM structures have i-CS(B) configurations for mid-range compositions. Consistent with the variation of structures, the variation in segregation type for parameter sets ***I*** and ***II*** is dominated by the composition dependendence, while potential parameter effects are dominant for parameter set ***III*** (Fig. 4(c)), which exhibits a wider range of segregation types, with the most stable configuration (M) changing from spherical cap ($w_a$ = 0.0–0.1), to i-CS(A) ($w_a$ = 0.2–0.7) and mixed ($w_a$ = 0.8–1.0).

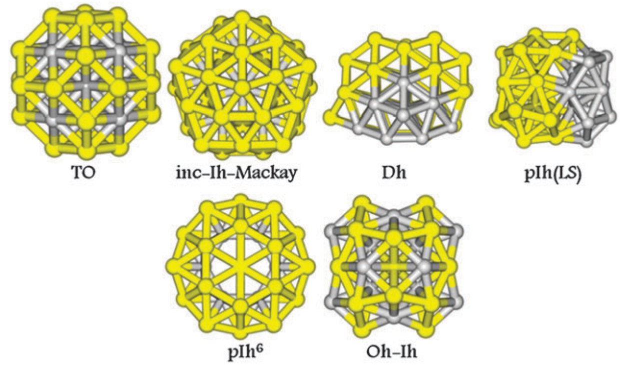


**Fig. 5** GM structural motifs found for PdAu-38.

### 3.2 38-Atom palladium–gold clusters

GA calculations for 38-atom clusters very often present truncated octahedra (TO) as the preferred structure.[25] In a previous study of 38-atom Pd–Au clusters, TO structures were found to be the GM for all compositions when using the **average** potential, and to predominate for the **DFT-fit** and **exp-fit** potentials.[11] TO structures of Pd–Au typically have Au atoms segregated to the surface and Pd atoms occupying core positions, though the **DFT-fit** and **exp-fit** potentials give rise to more surface Pd–Au mixing than the **average** potential.

In this study, the TO structure is again found to predominate for parameter sets ***I–III***. However, by varying the parameters of the Gupta potential, other structures are found to be competitive; incomplete Mackay-icosahedra (inc- Ih-Mackay), decahedra (Dh), low symmetry-polyicosahedra (pIh(LS)), six-fold symmetric polyicosahedra (pIh$^6$)[41] and mixed octahedra–icosahedra (Oh–Ih)[25] (see Fig. 5).

**Energetics and structural motifs.** Fig. 6 shows the variation of the Gupta excess energy $\Delta_{38}^{\mathrm{Gupta}}$ as a function of composition and weighting factor for parameter sets ***I–III***. Fig. 6(a) shows that, except for $w$ = 0.0 at compositions (2,36) and (1,37), all the other GM for parameter set ***I*** exhibit Pd–Au mixing. A similarity between the excess energy profiles of 34- and 38-atom clusters for parameter set ***I*** is the occurrence of crossings of the excess energy curves (for different weighting factors) from mid-range to Pd-rich compositions. All GM in the range $w$ = 0.0 to 0.8 are TO, with inc-Ih-Mackay only competitive for Pd-biased weighted parameters in the composition range (10,28) to (5,33).

Several straight line regions are evident from the plotted excess energies that were not found for the 34-atom clusters. The first straight line region is from the pure-Pd composition (38,0) to composition (26,12), after which more gradual changes of excess energy correspond to the formation of new Au–Au bonds on the surface of the cluster, as shown in Fig. 7(a) (substitution of 1–12 Au atoms into $Pd_{38}$ for $w_a$ = 0.0–0.2 only introduces heteronuclear Pd–Au interactions). The next straight line region commences at composition (14,24) (Fig. 7(b)), after which point Au atoms start to occupy the centroids of the (111) facets on the cluster surfaces. The transition from 12 to 13 Au atoms and from 24 to 25 Au atoms specifically shows how Au prefers (100) sites, leaving Pd on (111) facets, consistent with the findings of DFT

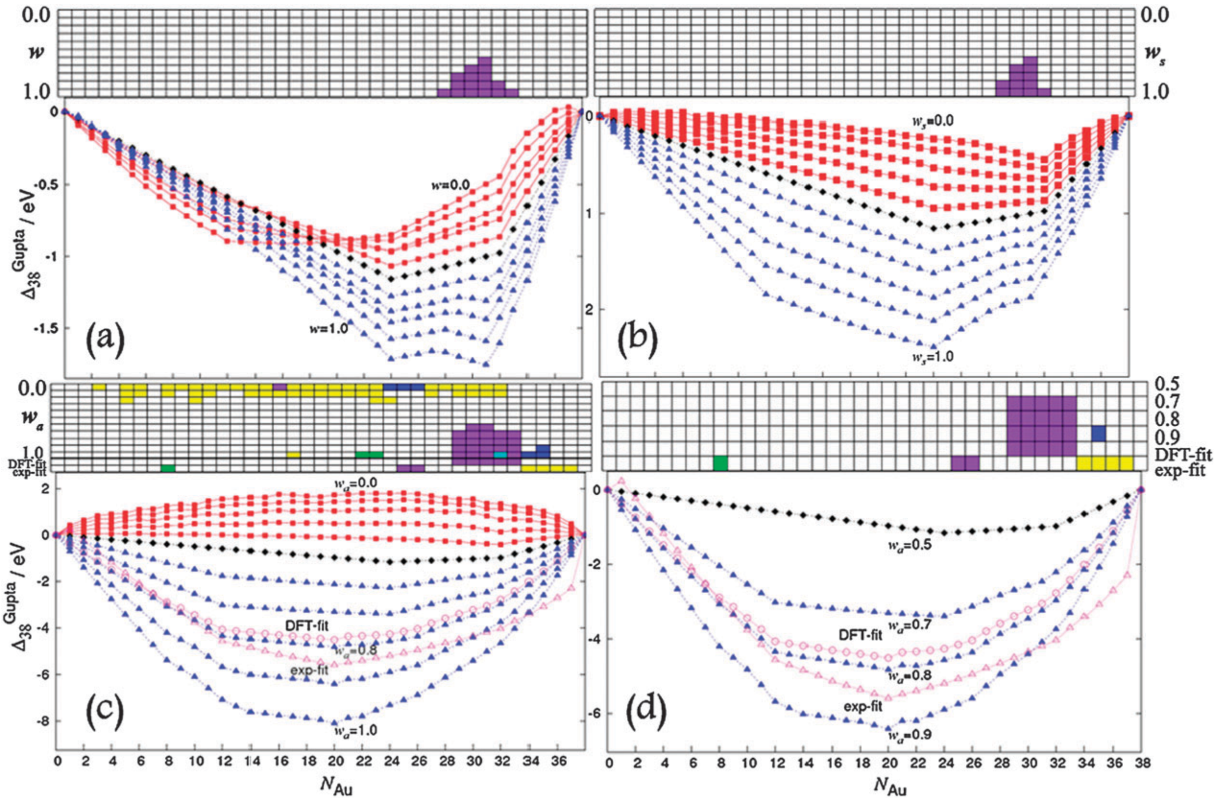


**Fig. 6** (Bottom) Excess energy variation ($\Delta_{38}^{\mathrm{Gupta}}$) for 38-atom Pd–Au clusters using parameter sets ***I*** (a), ***II*** (b), and ***III*** (c). (d) is a comparison between set ***III*** ($w_a$ = 0.5,0.7–0.9) and the **DFT-fit** and **exp-fit** potentials. (Top) GM Structural motifs found, as a function of composition (number of Au atoms) and weighting factor ($w$, $w_s$ or $w_a$): TO (white); inc-Ih-Mackay (purple); Dh (yellow); pIh[LS] (blue); Oh–Ih (green); $pIh^6$ (cyan).

calculations.[51] This behaviour, also observed for $Au_{55}$, $Au_{98}$, $Au_{79}$, and $Au_{92}$, is promoted because of the stronger Pd–Au bond compared to either Au–Au or Pd–Pd bonds.[52] Subsequent transitions with large jumps of energy for compositions (6–32) to (5,33), correspond to Au atoms starting to occupy the inner cluster core, as shown in Fig. 7(c). For $w$ = 0.6–1.0, an almost identical transition occurs as a result of the structure changing from a pIh with 7 interior Pd atoms into a TO with 6 interior Pd atoms (Fig. 7(d)).

Using parameter set ***II*** (Fig. 6(b)), the excess energy plot shows no crossings for different weighting factors but the structural motifs are almost the same as for set ***I***. The same straight lines and transition-points are also observed.

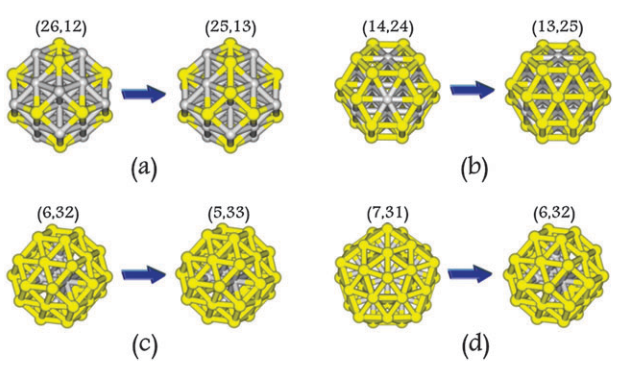


**Fig. 7** Configurational changes in PdAu-38 using parameter set ***I***: (a) 12Au to 13Au; (b) 24Au to 25Au; (c) 32Au to 33Au; and (d) structural change from 31Au to 32Au.

For parameter set ***III*** (Fig. 6(c)), Pd–Au mixing is not favourable (the excess energy is positive) for $w_a$ = 0.0–0.3 and also for Pd-rich ($N_{Au}$ = 1–12) clusters at $w_a$ = 0.4. Straight line regions can again be seen, with transitions at compositions (26,12) (for $w_a$ = 0.6–0.8) and (14,24) (for $w_a$ = 0.6–0.7), which are correlated with the introduction of new Au–Au bonds on the surface and the establishment of complete 7 Au-atom hexagonal (111) faces of the clusters, respectively, and are also observed for parameter sets ***I*** and ***II***. The most stable cluster for parameter set ***III*** at $w_a$ = 1.0 ($Pd_{18}Au_{20}$) has an excess energy of −8.1008 eV, which is much lower than for set ***I*** (−1.7552 eV for $Pd_7Au_{31}$) and set ***II*** (−2.3922 eV for $Pd_{14}Au_{24}$). The more negative excess energies for 38-atom Pd–Au clusters, using parameter set ***III***, are consistent with the results for the 34-atom clusters, and indicates an increase in the proportion of heteronuclear Pd–Au bonds in the cluster, which is favoured by the asymmetric weighting.

Overall, TO were found to be the most stable structures for set ***III***, except for low $w_a$ (0.0–0.1), where Dh structures dominate. For larger $w_a$ (0.6–1.0), inc-Ih-Mackay is a competitive structure, especially in the Au-rich range from (9,29) to (5,33). Other structures that might be competitive for Pd–Au clusters are $pIh^6$ ($w_a$ = 1.0,(6,32)), pIh(LS) and the new structures of Oh–Ih ($w_a$ = 1.0, (16,22) and (15,23)) that were not found previously for the **average** Gupta potential.[11,25] For $w_a$ = 0.8–1.0, the minima in excess energy occur at (18,20), after which there is a sudden increase of energy that can be explained by adding a single Au atom to the unfavourable core of the TO cluster.

Similar to the results for the 34-atom clusters, the variation of structures in the 38-atom Pd–Au clusters for parameter set ***I*** (Fig. 6(a)) and parameter set ***II*** (Fig. 6(b)) is mainly affected by the composition effect, in which the inc-Ih-Mackay structure is found as the putative GM for Au-rich compositions for weightings biased towards Pd (high $w$ and $w_s$). Moving to parameter set ***III*** (Fig. 6(c)), the composition effect still plays a role in intermediate parameterisation (close to the average), but the emergence of Dh and pIh[LS] structures (at low $w_a$) and Oh–Ih and pIh[6] structures (at high $w_a$) clearly shows the large effect of varying the parameter weighting for set ***III***.

For the **DFT-fit** potential, the excess energy plot for 38-atom Pd–Au clusters is consistent with that for 34 atoms; it is located between $w_a$ = 0.7 and 0.8 of parameter set ***III*** (Fig. 6(d)). The structural motifs are also in line with this trend, showing the same GM for all compositions. On the other hand, the **exp-fit** excess energy plot dips down below $w_a$ = 0.8 and at some points (for very rich Au compositions) the GM of this potential are more stable than the extreme parameters of set ***III*** ($w_a$ = 0.9–1.0). In terms of structural motifs, as for the 34-atom clusters, the **exp-fit** potential gives a totally different composition variation compared to the GM of set ***III***. Along with the dominant TO, other structures from the **exp-fit** potential calculations are Dh [(4,34) to (1,37)], inc-Ih-Mackay [(13,25) and (12,26)] and Oh–Ih [(30,8)]; with the latter structure also found at $w_a$ = 1.0 for set ***III***.

**GM structural variation and segregation profiles.** Fig. 8(a) shows TO ($w$ = 0.0–0.8) and inc-pIh-Mackay ($w$ = 0.9–1.0) structures have the most negative excess energies for parameter set ***I***. However, if just $A$ and $\xi$ are varied in a symmetrical manner (set ***II***) (Fig. 8(b)) then the lowest excess energies only correspond to TO, either with composition (6,32) ($w_s$ = 0.0–0.3) or (14,24) ($w_s$ = 0.4–1.0). Parameter set ***III*** (Fig. 8(c)) has a pIh(LS) structure as the lowest excess energy for $w_a$ = 0.0, followed by a range of TO structures with different compositions for $w_a$ = 0.1–0.7, and the most negative excess energies of all are distorted-TO (towards Oh–Ih) for $w_a$ = 0.8–1.0.

Similar to parameter set ***III*** ($w_a$ = 0.8 and 0.9), the lowest excess energy structures for the **DFT-fit** and **exp-fit** potentials have composition (18,20) with structures which are TO distorted towards Oh–Ih, as shown in Fig. 8(d). It should be noted that mixed Oh–Ih motifs can only be found at very Pd-rich compositions, *i.e.* (30,8) for the **exp-fit** potential, and also for set ***III*** (with $w_a$ = 1.0) at compositions (16,22) and (15,23). For medium compositions, it shows a similar type of structure (TO distorted towards Oh–Ih) with core–shell chemical ordering. Compared to 34-atom clusters,[26] 38-atom Pd–Au clusters do not exhibit a rich diversity of structures and segregation, but this size produces stable TO structures—which is a fragment of fcc packing—as in the bulk phases of pure palladium and gold.[5,7]

The segregation profiles in Fig. 9 agree with our earlier observations, showing a tendency towards TO structures having Au atoms segregated to the surface and Pd atoms occupying core positions.[25] All the minimum excess energy isomers (M) (for all weighting factors) for parameter sets ***I*** (Fig. 9(a)) and ***II*** (Fig. 9(b)) display i-CS(C) chemical ordering, with all Au atoms on the surface. This is in agreement with experimental[11,42] and other theoretical studies.[45] In addition to a wide range (in composition and weighting) of stability of the i-CS(A) configuration, i-CS(C) emerges as a favourable configuration for Pd-rich clusters for parameter sets ***I*** (low $w$) and ***II*** (high $w_s$). Compared to the 34-atom clusters, 38-atom PdAu clusters with TO geometries show stronger evidence of the tendency of Au atoms to occupy the sites with the lowest coordination—*i.e.* the square (100) facet sites—leaving Pd atoms at the centres of the hexagonal (111) facets. The ionic contribution to the Pd–Au bonding plays a role in promoting a large number of Pd–Au bonds on the surface compared to Pd–Pd and Au–Au bonds,[25,51,52] resulting in a strong dominance of i-CS(A) configurations for parameter set ***I*** and ***II***. The strength of the slightly ionic Pd–Au bond is increased by electron transfer from the Pd atom to the region between Au and Pd, which is due to the slightly larger Pauling electronegativity of Au (2.54) than that of Pd (2.20).[53] The i-CS(A) and i-CS(C) configurations were observed previously with the **average** parameter set for 38-atom $Pd_{core}Au_{shell}$ clusters,[25] as well as for $Ni_{core}Ag_{shell}$,[49] $Au_{core}Ag_{shell}$ and $Pt_{core}Pd_{shell}$[54] clusters, and agrees with the observation of isolated Pd surface sites surrounded by Au atoms in several experimental studies.[55–58]

As for the 34-atom Pd–Au clusters, $w_s$ = 0.0 is found to generate GM with i-CS(B) configurations. Interestingly, 38-atom Pd–Au clusters exhibit this type of segregation over a wider composition range, and also for $w_s$ = 0.1, with a ***type-B*—*type-A*** transition at $w_s$ = 0.1.

In contrast to parameter sets ***I*** and ***II***, chemical ordering of minimum excess energy structures (M) for parameter set ***III*** (Fig. 9(c)) varies from spherical cap ($w_a$ = 0.0) to ball-and-cup ($w_a$ = 0.1), i-CS(B) ($w_a$ = 0.2–0.3), complete core–shell ($w_a$ = 0.4) and i-CS(A) ($w_a$ = 0.5–1.0). Mixed clusters (with 1–4 Au atoms in the core), which are favoured over a wide range of compositions for $w_a$ = 0.8–1.0, do not have the lowest excess energies. Again, the crossover of chemical ordering for parameter set ***III*** indicates the dominance of parameterisation over composition effects (with composition dominating for parameter sets ***I*** and ***II***).

**Comparison of GM and metastable structured motifs.** In this paper, we mainly focus on the putative GM, as it would involve a very long discussion to include (even some of the) local minimum structures for all compositions of two cluster sizes (34 and 38 atoms) and for three parameterisation schemes (parameter sets ***I***, ***II*** and ***II***). However, a brief consideration of metastable structures is presented here.

A detailed study for all compositions of 38-atom Pd–Au clusters, using the average potential ($w$ = $w_a$ = $w_s$ = 0.5) (Fig. 10), shows that there is close competition between Dh, inc-Ih-Mackay and TO structures across the entire composition range, with pIh[6] being relatively unstable. TO are the putative GM found by the GA for all compositions.

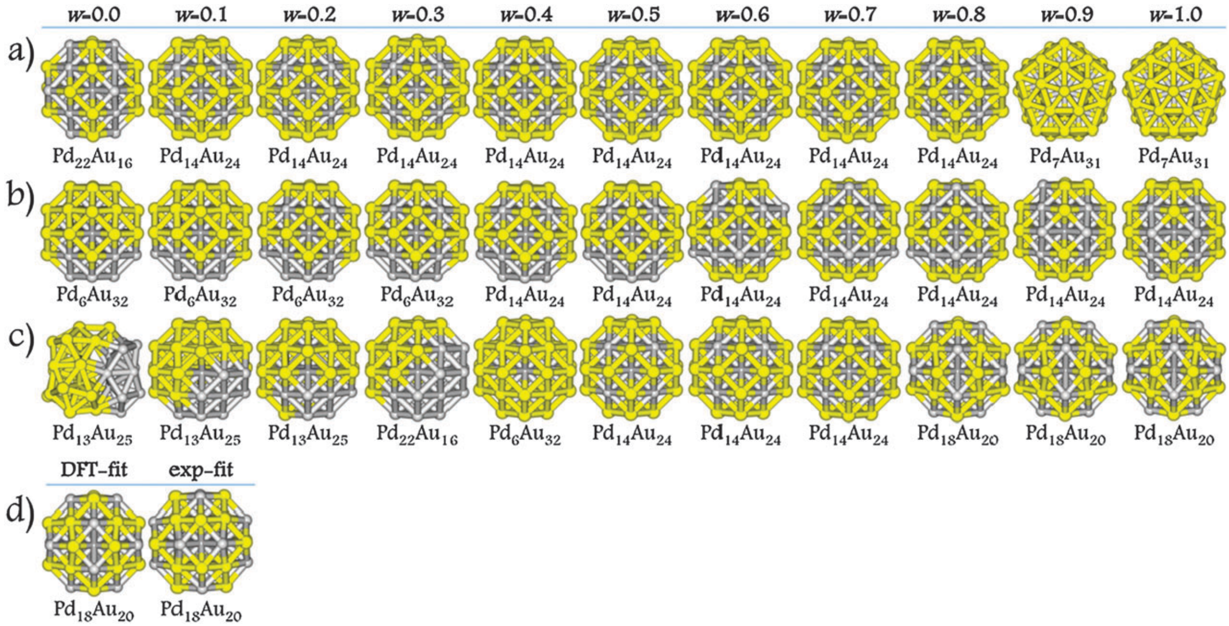


**Fig. 8** Structural variation of the lowest excess energy PdAu-38 isomers found for parameter sets ***I*** (a), ***II*** (b), ***III*** (c), and the **DFT-fit** and **exp-fit** potentials (d).

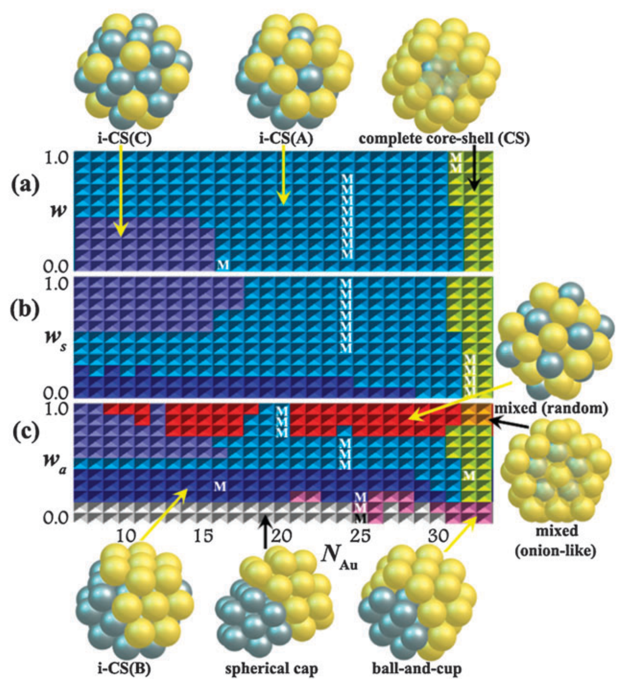


**Fig. 9** Segregation profiles of PdAu-38 using parameter sets ***I*** (a), ***II*** (b), and ***III*** (c).

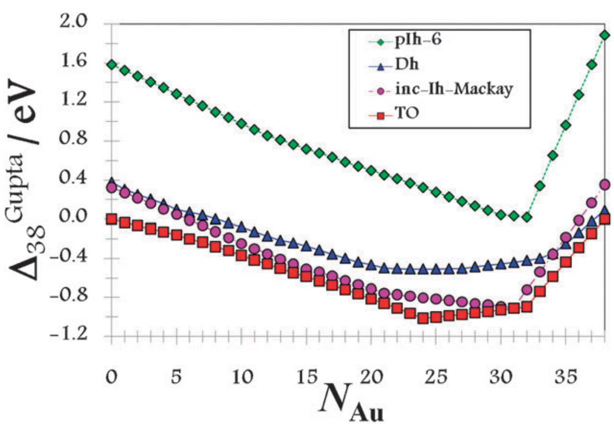


**Fig. 10** Composition-dependent variation of the excess energies of four structural motifs of 38-atom Pd–Au clusters using the **average** potential ($w$ = 0.5).

GA calculations for the fixed composition $Pd_6Au_{32}$, as a function of the weightings $w$, for parameter set ***I*** (Fig. 11(a)) give the TO as the GM for all weightings except $w$ = 0.9 and 1.0, for which the inc-Ih-Mackay structure is more stable. Parameter set ***II*** (Fig. 11(b)) gives inc-Ih-Mackay as the GM only for $w_s$ = 1.0. However, for parameter set ***III*** (Fig. 11(c)), the GM predicted varies significantly with weighting: Dh (with ball-and-cup segregation) ($w_a$ = 0.0–0.1); TO ($w_a$ = 0.2–0.6); inc-Ih-Mackay ($w_a$ = 0.7–0.9); and $pIh^6$ ($w_a$ = 1.0). This shows the sensitivity of the Gupta potential to varying the potential parameters, especially for parameter set ***III***.

### 3.3 Analysis of segregation in Pd–Au clusters

**Pair distribution function (PDF).** Based on the bulk fcc lattice, the nearest- and second-nearest neighbour distances are 2.7485 and 3.8479 Å for Pd and 2.8840 and 4.037 Å for Au, respectively. By examining each of the PDF plots, it was decided to select the values of 3.3 Å (Pd–Pd), 3.5 Å (Au–Au) and 3.4 Å (Pd–Au), as the cut-off for defining each respective type of bond. This is consistent with the bulk data ($r_{Pd–Pd} < r_{Pd–Au} < r_{Au–Au}$) and the bulk distances mentioned above. PDFs for 34-atom clusters are more complex than for the 38-atom clusters for all parameter sets, due to the greater bond length distribution variation of the structural families.

 

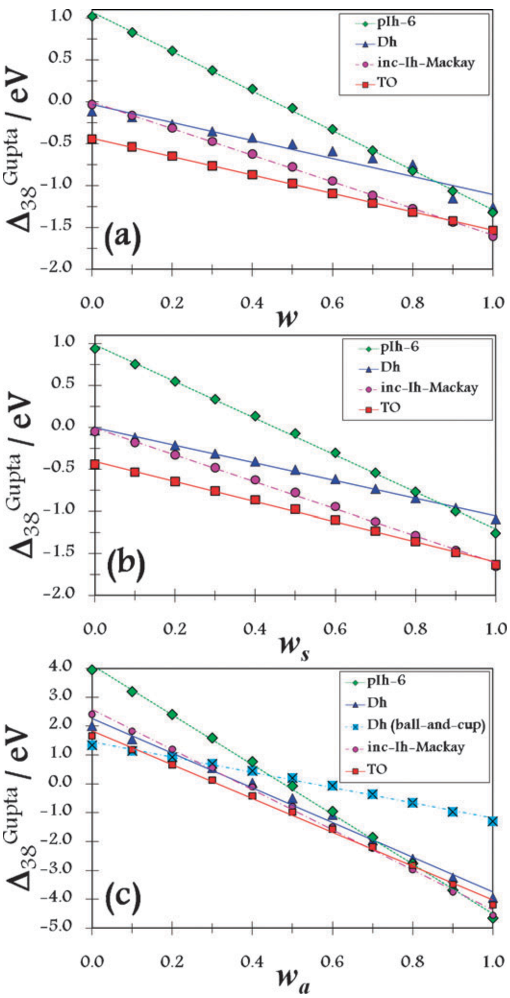


**Fig. 11** Parameter weighting-dependent variation of the excess energies of four structural motifs of $Pd_6Au_{32}$ using parameter sets ***I*** (a), ***II*** (b) and ***III*** (c).

**Average nearest neighbour distance (ANND).** Calculations on the GM derived from the GA search give ANNDs of pure Pd clusters of 2.6760 Å (34-atoms) and 2.6696 Å (38-atoms), while pure Au clusters display smaller values of 2.7932 Å (34-atoms) and 2.7886 Å (38-atoms). Consistent with previous research on Pd–Au clusters using the **average** potential ($w$ = 0.5 in this work), there is a steady increase in ANND with increasing Au content, due to the larger atomic radius of Au, in accordance with Vegard's law. Sudden changes in ANND are consistent with a change of structural motif.[11]

Due to the relatively small difference in the Gupta potential parameters between Pd and Au,[12] it is expected that ANND data for bimetallic clusters combining the two, would result in a straightforward pattern. However, moving from Au-biased parameters ($w = w_a = 0.0$) to Pd-biased parameters ($w = w_a = 1.0$) (Fig. 12(a), (b), (d) and (e)), there is a slight deviation of the curve, with a large plateau at Pd-rich compositions. This slow movement means that the ANND remains low (close to bulk Pd), in line with shifting towards Pd-biased Gupta parameters. The antisymmetric weighting potential for PdAu-34 (Fig. 12(c)) shows more fluctuation, in agreement with the heterogeneous pIh structures, compared to continual

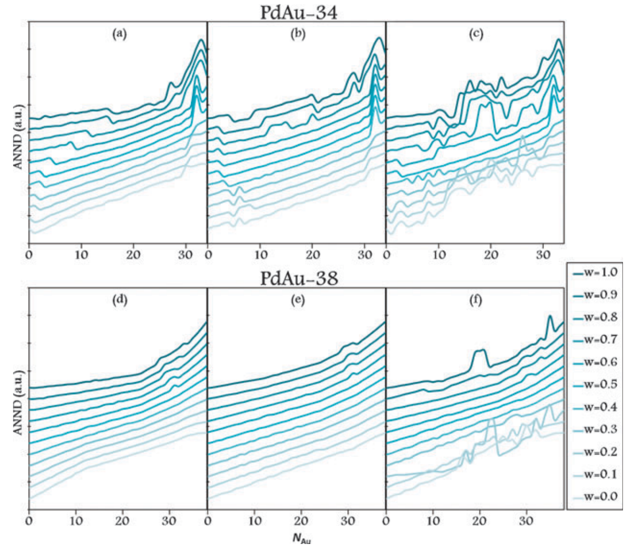


**Fig. 12** ANND variation for PdAu-34 using parameter sets ***I*** (a), ***II*** (b), and ***III*** (c) and for PdAu-38 using sets ***I*** (d), ***II*** (e), and ***III*** (f).

TO structures of PdAu-38 (Fig. 12(f)). The ANNDs for parameter set ***III***, with high values of $w_a$, exhibit a high degree of Pd–Au mixing, similar to the **DFT-fit** and **exp-fit** potentials reported earlier with jagged behaviour of ANNDs.[11]

**Chemical order.** An earlier study of 38-atom Pd–Au clusters using the **average** Gupta parameters ($w$ = 0.5) showed that the chemical order parameter, $\sigma$, has positive values for all compositions, with minima ($\sigma$ = 0) at $Pd_{15}Au_{23}$ and $Pd_{14}Au_{24}$.[11] These positive $\sigma$ values correspond to core–shell segregation. For PdAu-34 clusters, the lowest $\sigma$ value occurs at $Pd_{14}Au_{20}$, and is more positive than for PdAu-38, with all compositions again having positive $\sigma$ values, corresponding to core–shell segregation.

Using parameter set ***I***, PdAu-34 (Fig. 13(a)) does not show significant differences compared to the **average** potential ($w$ = 0.5). In contrast, 38-atom Pd–Au clusters (Fig. 13(d)) exhibit better mixing at $w$ = 0.6–1.0, specifically for medium compositions. Parameter set ***II*** shows some increase in mixing for PdAu-34 (Fig. 13(b)), but is consistent with set ***I*** for PdAu-38 (Fig. 13(e)). Interestingly, parameter set ***III*** reveals considerable deviations from the **average** potential results. PdAu-34 clusters (Fig. 13(c)) possess $\sigma$ values close to zero ($w_a$ = 0.6) and negative values ($w_a$ = 0.7–1.0), indicating a higher degree of mixing. For PdAu-38 clusters (Fig. 13(f)) negative $\sigma$ values are only found over a wide composition range for $w_a$ = 0.8–1.0. This is consistent with previous calculations on 38-atom Pd–Au clusters using the **DFT-fit** and **exp-fit** potentials. Consistent with other analyses, parameter set ***III*** displays the largest variation from the **average** potential curve ($w = w_s = w_a = 0.5$). Biasing the parameters towards higher $w_a$ (> 0.5) leads to increased Pd–Au mixing, as shown by the increased number of Pd–Au bonds relative to homonuclear bonds, and hence the more negative values of $\sigma$. At $w_a$ = 1.0, the tendency to form mixed bonds distorts the clusters towards an ordered mixing arrangement. For PdAu-34 a distorted bcc/Dh structure is adopted at composition

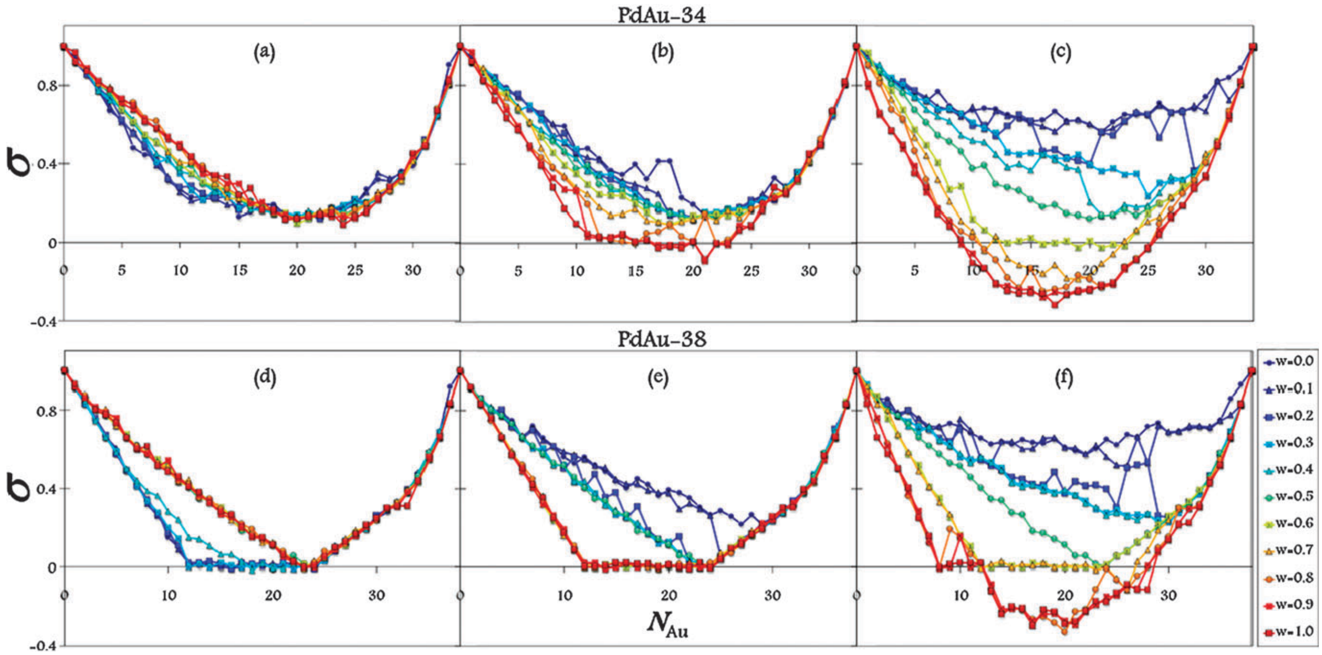


**Fig. 13** Chemical order parameter ($\sigma$) for PdAu-34 using parameter sets ***I*** (a), ***II*** (b), and ***III*** (c) and for PdAu-38 using sets ***I*** (d), ***II*** (e), and ***III*** (f).

(17,17), while for PdAu-38 the Oh–Ih motif is found as the GM at (16,22) and (15,23), rather than the TO structure.

## 4. Conclusions

A detailed discussion of the energetics, structures and segregation of Pd–Au nanoalloy clusters has been presented, for 34- and 38-atom Pd–Au clusters, using three types of heteronuclear potential parameterisation. Parameter set ***I*** (in which all parameters in the Gupta potential are weighted symmetrically) and parameter set ***II*** (where only the energy-scaling parameters $A$ and $\xi$ are varied, with the remaining parameters kept at their average values) give very slight variation in structures, with the ordering being dominated by changes in elemental composition. However a clear dependence of structure on parameter weighting is observed for parameter set ***III*** (antisymmetric variation of $A$ and $\xi$).

The in-depth structural analysis of 34-atom clusters showed Dh, pIh and TO structural motifs as the putative global minima, while the TO structure faces competition from inc-Ih-Mackay, Dh, pIh(LS), pIh[6] and Oh–Ih for 38-atom clusters. Generally, the new Oh–Ih configuration ($w_a$ = 1.0, (16,22) and (15,23)) was not found as a GM for the **average** Gupta potential, but it has been found as the lowest-energy isomer for Ag–Pt clusters at the DFT level.[25] These results show that, by finely tuning the Gupta potential, it is possible to qualitatively reproduce the results observed at higher levels of theory.

The significant crossover of chemical ordering type (core–shell, spherical cap, ball-and-cup and mixed) observed for parameter set ***III*** also indicates that parameter weighting dominates composition effects for this parameter set. Chemical ordering of the GM are consistent with the ANND and sigma ($\sigma$) profiles, in which parameter set ***III*** displays an evolution of structural families towards an ordered mixing arrangement (the distorted bcc/Dh structure for PdAu-34 and Oh–Ih for PdAu-38) for higher $w_a$ values ($>0.5$).

Comparing the results from parameter set ***III*** and the fitted (**DFT-fit** and **exp-fit**) potentials generated some interesting conclusions. Parameter set ***III*** with $w_a > 0.5$ gave stronger Pd–Au bonding, as shown by the more negative excess or mixing energies for both cluster systems. This weighting scheme results in less Pd–Au repulsion ($A_{PdAu} \rightarrow A_{Pd}$) and more Pd–Au attraction ($\xi_{PdAu} \rightarrow \xi_{Au}$) in the clusters. This is because $A_{Pd}$ (0.1746) $<$ $A_{Au}$ (0.2061) and $\xi_{Pd}$ (1.7180) $<$ $\xi_{Au}$ (1.7900); so that as $w_a \rightarrow 1.0$ the $A$ parameter (repulsion) is reduced and the $\xi$ parameter (attraction) increases. The **DFT-fit** potential gives more comparable results to those of parameter set ***III***. The **DFT-fit** potential has the following characteristics which are similar to those in the antisymmetric (set ***III***) weighted Gupta potential: $A_{\text{DFT-fit}}$ (0.1843) $\sim$ $A_{w_a} = 0.7$ (0.1841) and $\xi_{\text{DFT-fit}}$ (1.7867) $\sim$ $\xi_{w_a} = 0.9$ (1.7828). These correlations are consistent with the overall results for 34- and 38-atom PdAu clusters, that show the **DFT-fit** potential giving similar results of excess energies and lowest energy structures and homotops to those for $w_a$ = 0.8. The **exp-fit** potential also gives similar excess energies to the results for $w_a$ = 0.8, though the shape of the curve is a little different—but the structures and homotops are often quite different to the results from parameter set ***III***. This is not surprising, since, as noted previously,[11] the **exp-fit** parameters are qualitatively very different. In particular we note that for the **exp-fit** potential: $A_{PdAu} > A_{PdPd}$ and $A_{AuAu}$; $\xi_{PdAu} > \xi_{PdPd}$ and $\xi_{AuAu}$.

We have shown, therefore, that a simple asymmetrical weighting (parameter set ***III***) of the Pd–Au pair ($A$) and many-body ($\xi$) energy scaling parameters in the Gupta potential can qualitatively reproduce the energetic, structures and chemical ordering of the **DFT-fit** potential. As the next step in this research, we will select new, low-energy structures and homotops arising from set ***III*** that were not found in previous work[11] and we will carry out DFT re-minimisations in order to evaluate how they compare with those obtained previously. Finally, since it is known that the Gupta potential typically underestimates bulk surface energies,[3] in future work, we will also address the effect of modifying the potential, so as to reproduce Pd, Au and Pd–Au surface energies accurately, on the structures and chemical ordering of Pd–Au clusters.

## Acknowledgements

RI is grateful to Universiti Pendidikan Sultan Idris and the Ministry of Higher Education (Malaysia) for the award of a PhD scholarship. Calculations were performed on the University of Birmingham's BueBEAR high-performance computer.[59] The authors acknowledge Profs Riccardo Ferrando and Alessandro Fortunelli for helpful discussions and RI is grateful to Dr Oliver Paz-Borbón for his initial help in running the BCGA program.

## References

1 R. L. Johnston, *Atomic and Molecular Clusters*, Taylor & Francis, London, 2002.
2 T. P. Martin, *Phys. Rep.*, 1996, **273**, 199.
3 F. Baletto and R. Ferrando, *Rev. Mod. Phys.*, 2005, **77**, 371.
4 R. Ferrando, J. Jellinek and R. L. Johnston, *Chem. Rev.*, 2008, **108**, 845.
5 D. Schebarchov and S. Hendy, *Phys. Rev. B: Condens. Matter Mater. Phys.*, 2006, **73**, 121402.
6 M. José-Yacamán, M. Marín-Almazoc and J. A. Ascencio, *J. Mol. Catal. A: Chem.*, 2001, **173**, 61.
7 D. M. P. Mingos, *J. Chem. Soc., Dalton Trans.*, 1996, 561.
8 J. A. Ascencio, C. Gutiérrez-Wing, M. E. Espinosa, M. Marín, S. Tehuacanero, C. Zorrilla and M. José-Yacamán, *Surf. Sci.*, 1998, **396**, 349.
9 C. L. Cleveland, U. Landman, T. G. Schaaff, M. N. Shafigullin, P. W. Stephens and R. L. Whetten, *Phys. Rev. Lett.*, 1997, **79**, 1873.
10 H. B. Liu, U. Pal, A. Medina, C. Maldonado and J. A. Ascencio, *Phys. Rev. B: Condens. Matter Mater. Phys.*, 2005, **71**, 075403.
11 F. Pittaway, L. O. Paz-Borbón, R. L. Johnston, H. Arslan, R. Ferrando, C. Mottet, G. Barcaro and A. Fortunelli, *J. Phys. Chem. C*, 2009, **113**, 9141.
12 F. Cleri and V. Rosato, *Phys. Rev. B: Condens. Matter*, 1993, **48**, 22.
13 A. F. Lee, C. J. Baddeley, C. Hardacre, R. M. Ormerod, R. M. Lambert, G. Schmid and H. West, *J. Phys. Chem.*, 1995, **99**, 6096.
14 H. Bönnemann, U. Endruschat, B. Tesche, A. Rufïnska, C. W. Lehmann, F. E. Wagner, G. Filoti, V. Pârvulescu and V. I. Pârvulescu, *Eur. J. Inorg. Chem.*, 2000, 819.
15 V. I. Pârvulescu, V. Pârvulescu, U. Endruschat, G. Filoti, F. E. Wagner, C. Kübel and R. Richards, *Chem.–Eur. J.*, 2006, **12**, 2343.
16 E. Gross, I. Popov and M. Asscher, *J. Phys. Chem. C*, 2009, **113**, 18341.
17 M. O. Nutt, J. B. Hughes and M. S. Wong, *Environ. Sci. Technol.*, 2005, **39**, 1346.
18 N. Toshima, T. Yonezawa and K. Kushiashi, *J. Chem. Soc., Faraday Trans.*, 1993, **89**, 2537.
19 J. K. Edwards, B. E. Solsona, P. Landon, A. F. Carley, A. Herzing, C. J. Kiely and G. J. Hutchings, *J. Catal.*, 2005, **236**, 69.
20 D. I. Enache, J. K. Edwards, P. Landon, B. Solsona-Espriu, A. F. Carley, A. A. Herzing, M. Watanabe, C. J. Kiely, D. W. Knight and G. Hutchings, *Science*, 2006, **311**, 362.
21 D. H. Turkenburg, A. A. Antipov, M. B. Thathagar, G. Rothenberg, G. B. Sukhorukov and E. Eiser, *Phys. Chem. Chem. Phys.*, 2005, **7**, 2237.
22 Y. F. Han, J. H. Wang, D. Kumar, Z. Yan and D. W. Goodman, *J. Catal.*, 2005, **232**, 467.
23 M. Chen, D. Kumar, C. W. Yi and D. W. Goodman, *Science*, 2005, **310**, 291.
24 L. O. Paz-Borbón, A. Gupta and R. L. Johnston, *J. Mater. Chem.*, 2008, **18**, 4154.
25 L. O. Paz-Borbón, R. L. Johnston, G. Barcaro and A. Fortunelli, *J. Chem. Phys.*, 2008, **128**, 134517.
26 L. O. Paz-Borbon, R. L. Johnston, G. Barcaro and A. Fortunelli, *J. Phys. Chem. C*, 2007, **111**, 2936.
27 R. P. Gupta, *Phys. Rev. B: Condens. Matter*, 1981, **23**, 6265.
28 C. Massen, T. V. Mortimer-Jones and R. L. Johnston, *J. Chem. Soc., Dalton Trans.*, 2002, 4375.
29 A. J. Renouprez, J. L. Rousset, A. M. Cadrot, Y. Soldo and L. Stievano, *J. Alloys Compd.*, 2001, **328**, 50.
30 J. L. Rousset, L. Stievano, F. J. Cadete Santos Aires, C. Geantet, A. J. Renouprez and M. Pellarin, *J. Catal.*, 2001, **202**, 163.
31 D. Bazin, D. Guillaume, C. Pichon, D. Uzio and S. Lopez, *Oil Gas Sci. Technol.*, 2005, **60**, 801.
32 A. Fortunelli and G. Barcaro, personal communication.
33 R. Ismail and R. L. Johnston, unpublished work.
34 R. Hultgren, P. D. Desai, D. T. Hawkins, M. Gleiser and K. K. Kelley, *Values of the Thermodynamic Properties of Binary Alloys*, American Society for Metals, Metals Park, Ohio, 1973.
35 R. L. Johnston, *Dalton Trans.*, 2003, 4193.
36 M. M. Mariscal, N. A. Oldani, S. A. Dassie and E. P. M. Leiva, *Faraday Discuss.*, 2008, **138**, 89.
37 L. B. Hansen, P. Stoltze, J. K. Norskov, B. S. Clausen and W. Niemann, *Phys. Rev. Lett.*, 1990, **64**, 3155.
38 M. Itoh, V. Kumar, T. Adschiri and Y. Kawazoe, 2009, arXiv:0902.0080.
39 J. Jellinek and E. B. Krissinel, *Theory of Atomic and Molecular Clusters*, Springer-Verlag, Berlin, 1999.
40 F. Aguilera-Granja, A. Vega, J. Rogan, X. Andrade and G. Garcia, *Phys. Rev. B: Condens. Matter Mater. Phys.*, 2006, **74**, 224405.
41 G. Rossi, A. Rapallo, C. Mottet, A. Fortunelli, F. Baletto and R. Ferrando, *Phys. Rev. Lett.*, 2004, **93**, 105503.
42 J. L. Rousset, J. C. Bertolini and P. Miegge, *Phys. Rev. B: Condens. Matter*, 1996, **53**, 4947.
43 M. Mandal, S. Kundu, S. K. Ghosh and T. J. Pal, *J. Photochem. Photobiol., A*, 2004, **167**, 17.
44 A. Henglein, *J. Phys. Chem. B*, 2000, **104**, 6683.
45 H. B. Liu, U. Pal, A. Medina, C. Malonado and J. A. Ascencio, *Phys. Rev. B: Condens. Matter Mater. Phys.*, 2005, **71**, 075403.
46 H. B. Liu, U. Pal, R. Perez and J. A. Ascencio, *J. Phys. Chem. B*, 2006, **110**, 5191.
47 W. R. Tyson and W. A. Miller, *Surf. Sci.*, 1977, **62**, 267.
48 A.R. Miedema, *Z. Metallkd.*, 1978, **69**, 287.
49 A. Rapallo, G. Rossi, R. Ferrando, A. Fortunelli, B. C. Curley, L. D. Lloyd, G. M. Tarbuck and R. L. Johnston, *J. Chem. Phys.*, 2005, **122**, 194308.
50 D. T. Tran and R. L. Johnston, *Phys. Chem. Chem. Phys.*, 2009, **11**, 10340.
51 D. Yuan, X. Gong and R. Wu, *Phys. Rev. B: Condens. Matter Mater. Phys.*, 2007, **75**, 085428.
52 D. Yuan, X. Gong and R. Wu, *Phys. Rev. B: Condens. Matter Mater. Phys.*, 2008, **78**, 035441.
53 J. E. Huheey, *Inorganic Chemistry: Principles of Structure and Reactivity*, Harper & Row, New York, 1983.
54 G. Rossi, R. Ferrando, A. Rapallo, A. Fortunelli, B. C. Curley, L. D. Lloyd and R. L. Johnston, *J. Chem. Phys.*, 2005, **122**, 194309.
55 K. Luo, T. Wei, C. W. Yi, S. Axnanda and D. W. Goodman, *J. Phys. Chem. B*, 2005, **109**, 23517.
56 S. J. Mejia-Rosales, C. Fernandez-Navarro, E. Prez-Tijerina, D. A. Blom, L. F. Allard and M. Jose-Yacaman, *J. Phys. Chem. C*, 2007, **111**, 1256.
57 M. José-Yacamán, E. Pérez-Tijerina and S. J. Mejía-Rosales, *J. Mater. Chem.*, 2007, **17**, 1035.
58 C. W. Yi, K. Luo, T. Wei and D. W. Goodman, *J. Phys. Chem. B*, 2005, **109**, 18535.
59 http://www.bear.bham.ac.uk.